# Biochanin A inhibits endothelial dysfunction induced by IL-6-stimulated endothelial microparticles in Perthes disease via the NFκB pathway

JIANHONG LIU[1*], CHENGSEN LIN[1*], BOXIANG LI[2], QIAN HUANG[1], XIANXIANG CHEN[1], SHENGPING TANG[1], XIAOLIN LUO[1], RONGBIN LU[1], YUN LIU[1], SHIJIE LIAO[1,3] and XIAOFEI DING[1,3]

[1]Department of Orthopedic Trauma and Hand Surgery, The First Affiliated Hospital of Guangxi Medical University, Nanning, Guangxi Zhuang Autonomous Region 530021; [2]Department of Orthopedics, Minzu Hospital of Guangxi Zhuang Autonomous Region, Nanning, Guangxi Zhuang Autonomous Region 530001; [3]Guangxi Key Laboratory of Regenerative Medicine, Research Centre for Regenerative Medicine, Guangxi Medical University, Nanning, Guangxi Zhuang Autonomous Region 530021, P.R. China

**Abstract.** Endothelial dysfunction caused by the stimulation of endothelial microparticles (EMPs) by the inflammatory factor IL-6 is one of the pathogenic pathways associated with Perthes disease. The natural active product biochanin A (BCA) has an anti-inflammatory effect; however, whether it can alleviate endothelial dysfunction in Perthes disease is not known. The present *in vitro* experiments on human umbilical vein endothelial cells showed that 0-100 pg/ml IL-6-EMPs could induce endothelial dysfunction in a concentration-dependent manner, and the results of the Cell Counting Kit 8 assay revealed that, at concentrations of <20 $\mu$M, BCA had no cytotoxic effect. Reverse transcription-quantitative PCR demonstrated that BCA reduced the expression levels of the endothelial dysfunction indexes E-selectin and intercellular cell adhesion molecule-1 (ICAM-1) in a concentration-dependent manner. Immunofluorescence and western blotting illustrated that BCA increased the expression levels of zonula occludens-1 and decreased those of ICAM-1. Mechanistic studies showed that BCA inhibited activation of the NFκB pathway. *In vivo* experiments demonstrated that IL-6 was significantly increased in the rat model of ischemic necrosis of the femoral head, whereas BCA inhibited IL-6 production. Therefore, in Perthes disease, BCA may inhibit the NFκB pathway to suppress IL-6-EMP-induced endothelial dysfunction, and could thus be regarded as a potential treatment for Perthes disease.

## Introduction

Perthes disease, which results in the ischemic necrosis of the femoral epiphysis, mostly occurs in children aged 4-8 years with a worldwide incidence of 0.4-29.0/100,000 individuals <15 years of age. Notably, the incidence of this disease in male children is 4-5 times higher than that in female children (1,2). The most serious complication of Perthes disease is premature hip osteoarthritis caused by deformation of the femoral head (3). Conservative treatment using abduction plaster casts or inclusive surgery, which prevents secondary degenerative arthritis by maintaining the spherical shape of the femoral head and consistency in the femoral acetabular relationship, are adopted in clinical treatment; however, residual femoral head deformity remains inevitable in some patients, and can influence the normal development and physical and mental health of children. Although some researchers have attempted to treat this disease with drugs, such as zoledronic and ibandronate, it has achieved little effect (4,5).

The molecular mechanism underlying femoral head malformation in Perthes disease is still unclear, and may be related to endothelial dysfunction and abnormal vascular structure (6,7). IL-6 is a key pathogenic factor in Perthes disease. Kamiya *et al* (8) demonstrated that the concentration of the proinflammatory factor IL-6 in the hip synovial fluid of patients with Perthes disease is significantly elevated. By performing animal experiments, it was also revealed that the IL-6 receptor blocker can promote blood supply recovery to the femoral head epiphysis in Perthes disease (9). Endothelial microparticles (EMPs) are extracellular vesicles that are secreted by endothelial cells (10). When the body is in a pathological state, the secretion of EMPs increases, and the EMPs released by activated or apoptotic endothelial cells can

*Correspondence to:* Professor Xiaofei Ding or Dr Shijie Liao, Department of Orthopedic Trauma and Hand Surgery, The First Affiliated Hospital of Guangxi Medical University, 6 Shuangyong Road, Nanning, Guangxi Zhuang Autonomous Region 530021, P.R. China
E-mail: dxfeicsgk2014@163.com
E-mail: gxliaoshijie@163.com

*Contributed equally

reflect the degree of endothelial dysfunction (11). Our previous study (12) reported that the concentration of CD31$^+$/CD42b$^-$ EMPs is increased in the plasma of patients with Perthes disease and that this is related to the concentration of IL-6. Furthermore, CD31$^+$ EMPs produced by IL-6-stimulated human umbilical vein endothelial cells (HUVECs) *in vitro* can also induce endothelial dysfunction (12). On the basis of these findings, hypotheses have been made on whether drugs can inhibit this phenotype and alleviate the deformation of the femoral head in Perthes disease.

Biochanin A (BCA) is an oxygen-methylated isoflavone that exists in various herbs, such as Spatholobi Caulis, red clover, soy, chickpea and a number of other plants (13,14). Numerous studies have shown that BCA has pharmacological activities, such as anticancer (15), anti-inflammatory (16), neuroprotective (17), antioxidant (18), antimicrobial (19) and hepatoprotective (20) effects. Studies have also reported that BCA can reduce the expression of the inflammatory factor IL-6 and inhibit inflammation (21,22). Our previous study (23) revealed that BCA inhibits the NFκB signaling pathway to alleviate inflammatory responses in a murine calvaria model with osteolysis induced by Ti particle. Kole *et al* (24) also found that BCA can inhibit proinflammatory cytokines in mouse macrophage cell line. However, whether BCA inhibits IL-6-EMP-mediated endothelial dysfunction in Perthes disease via the NFκB signaling pathway remains to be determined.

The present study explored the effect and mechanism of BCA in IL-6-EMP-induced endothelial dysfunction through *in vitro* and *in vivo* experiments such as ELISA, immuno-fluorescence, reverse transcription-quantitative PCR, western blot and construction of rat model of femoral head ischemic necrosis.

**Materials and methods**

*Main equipment.* A multifunctional microplate reader and cell incubator were purchased from Thermo Fisher Scientific, Inc.; a cryogenic centrifuge was obtained from Eppendorf SE; an ultrahigh rotational speed centrifuge was from Beckman Coulter, Inc.; at -80˚C refrigerator was obtained from Haier Group; and the fluorescence inverted microscope was from Leica Microsystems GmbH.

*Main reagents.* RPMI-1640 medium, penicillin-streptomycin mixture and trypsin were from Gibco; Thermo Fisher Scientific, Inc.; fetal bovine serum (FBS) was purchased from Zhejiang Tianhang Biotechnology Co., Ltd.; BCA was obtained from Chengdu Desite Biotechnology Co., Ltd.; PBS, the Cell Counting Kit-8 (CCK-8), Dil fluorescent dye, Actin-Tracker Green-488, BCEBF-AM, SDS-PAGE sample loading buffer, BCA protein assay kit and IL-6 were purchased from Beyotime Institute of Biotechnology; the E-Selectin ELISA kit (cat. no. ml057603), vascular cell adhesion molecule-1 (VCAM-1) ELISA kit (cat. no. ml060757) and intercellular cell adhesion molecule-1 (ICAM-1) ELISA kit (cat. no. ml023955) was from Shanghai Enzyme-linked Biotechnology Co., Ltd.; DAPI was obtained from Sangon Biotech Co., Ltd.; sodium citrate buffer, DAB Substrate kit (20X), Hematoxylin-Eosin (HE) Stain kit, RIPA buffer (high),

phenylmethylsulfonyl fluoride (PMSF), protein phosphatase inhibitor, aprotinin from bovine lung and DMSO used to dissolve BCA was purchased from Beijing Solarbio Science & Technology Co., Ltd.; Bovine serum albumin (BSA) was purchased from Servicebio; 96-, 48- and 6-well cell culture plates and T75 and T25 cell culture flasks were from Corning, Inc.; E.Z.N.A.® Total RNA Kit I was purchased from Omega Bio-Tek, Inc.; RevertAid First Strand cDNA Synthesis kit was purchased from Thermo Fisher Scientific, Inc.; 2x SYBR Green PCR Mastermix was purchased from Thermo Fisher Scientific, Inc.; primary antibodies against ICAM-1 (cat. no. #4915), zonula occludens-1 (ZO-1; cat. no. #5406), NFκB (cat. no. #8242), IκB (cat. no. #4812) and VE-Cadherin (cat. no. #2500) for western blotting were purchased from Cell Signaling Technology, Inc; primary β-actin antibody (cat. no. GB15003) for western blot was purchased from Wuhan Servicebio Technology Co., Ltd.; primary ICAM-1 antibody (cat. no. #380990) for immunofluorescence and primary IL-6 antibody (cat. no. #500286) for immunohistochemical was purchased from Chengdu Zhengneng Biotechnology Co., Ltd.; primary ZO-1 antibody (cat. no. #AF5145) for immunofluores-cence was purchased from Affinity Biosciences; horseradish peroxidase-labeled goat anti-rabbit IgG secondary antibody (cat. no. A0208) for western blotting was purchased from Beyotime Institute of Biotechnology; Fluor594-conjugated goat anti-rabbit IgG secondary antibody (cat. no. #S0006) for immunofluorescence was purchased from Affinity Biosciences; West ECL was purchased from Hyczmbio; Universal two-step detection kit (cat. no. PV-9000) was purchased from OriGene Technologies, Inc.

*Cell culture.* The human umbilical vein endothelial cells (HUVECs) used in the present study were an immortalized cell line (cat. no. GDC0635), which was obtained from the China Center for Type Culture Collection. The cells were cultured in RPMI-1640 medium, supplemented with 10% FBS and 1% penicillin-streptomycin mixture, and were placed in a cell incubator containing 5% CO$_2$ at 37˚C. When the cells reached a confluence of 80-90% on the bottom of the T25 or T75 culture flasks, they were routinely digested and cultured in different culture flasks or plates in accordance with the experimental plan. The human monocyte cell line THP-1 was obtained from Procell Life Science & Technology Co., Ltd. THP-1 was cultured in RPMI-1640 complete medium obtained from Procell Life Science & Technology Co., Ltd., which contained 0.05 mM β-mercaptoethanol, 1% penicillin-streptomycin mixture and 10% FBS. The cells were placed in a cell incubator containing 5% CO$_2$ at 37˚C. The cells were passaged for 10 times when they had grown to a cell density of $1x10^6$ cells/ml.

*Extraction of EMPs.* HUVECs were cultured in T75 culture flasks. Briefly, the FBS used for HUVEC culture was centrifuged at 120,000 x g and 4˚C overnight to remove the extracellular vesicles contained therein. Various concentra-tions of IL-6 (0, 1, 10, 100 and 1,000 pg/ml) were added at room temperature after cell adherence and HUVECs were cultured at 37˚C for 24 h. When the cells had grown to ~90% confluence, the supernatant was gathered, centrifuged at 4˚C and 1,000 x g for 10 min, collected and centrifuged at

4˚C and 16,000 x g for 5 min, and collected and centrifuged again at 4˚C and 16,000 x g for 60 min. The supernatant was then discarded, and the EMPs were resuspended in 500 $\mu$l PBS and stored at -80˚C until further use (10).

*Endocytosis assay*. EMPs were incubated with the fluorescent dye Dil at 37˚C for 1 h, then they were centrifuged at 16,000 x g and 4˚C for 60 min. After discarding the supernatant, Dil-labeled EMPs were obtained. Dil-labeled EMPs were added to HUVECs for co-incubation at 37˚C for 4 h. At the end of the co-incubation, HUVECs were fixed with 4% paraformaldehyde at room temperature for 5 min and washed with 0.2% BSA-PBS three times. Then HUVECs were incubated with 0.3% Triton X-100 at room temperature for 5 min, incubated with 3% BSA-PBS at room temperature for 30 min and washed again with 0.2% BSA-PBS three times. HUVECs were stained with Actin-Tracker Green-488 at room temperature for 1 h and DAPI at room temperature for 10 min. At last, the cells were washed with PBS three times, observed under a fluorescence microscope and images were captured.

*Adhesion assay*. After routine digestion, HUVECs were cultivated in 96-well culture plates at a density of $3x10^3$ cells/well. After cell adhesion, HUVECs were treated with various concentrations of IL-6-EMPs (0, 1, 10, 100 or 1,000 pg/ml) or 100 pg/ml IL-6-EMPs plus different concentrations of BCA (0, 5 or 10 $\mu$M) at 37˚C for 24 h. The human monocytic cell line THP-1 was stained with BCECF-AM at 37˚C at a final concentration of 10 $\mu$M for 2 h. Subsequently, $1.5x10^4$ THP-1 cells/well were added to 96-well culture plates for 6-8 h of co-culture with HUVECs. At the end of the co-culture, the cells were washed with 1X PBS three times, observed under a fluorescence microscope and images were captured.

*CCK8*. After routine digestion, HUVECs were cultivated in 96-well culture plates at the density of $3x10^3$ cells/well. After cell adhesion, different concentrations of IL-6-EMPs (0, 1, 10, 100 and 1,000 pg/ml) and/or different concentrations of BCA (0, 2.5, 5, 10, 20 and 40 $\mu$M) were added to the plates. The plates were then incubated for 24 h in a 37˚C incubator containing 5% $CO_2$, after which, 10 $\mu$l CCK8 reagent/well was added and the cells were incubated at 37˚C for 2 h in the dark. The optical density (OD) of each well was measured at a wavelength of 450 nm, which represents the viability of the cells.

*ELISA*. After routine digestion, HUVECs were cultivated in 6-well culture plates at a density of $1x10^5$ cells/well. Different concentrations of IL-6-EMPs (0, 1, 10, 100 and 1,000 pg/ml) were added, and the supernatant was collected after 24 h of intervention at 37˚C. Subsequently, 10 $\mu$l supernatant and 40 $\mu$l diluent in the kit were added per well of a 96-well ELISA plate and the plate was incubated for 1 h at 37˚C in the dark. A total of 100 $\mu$l HRP-conjugated reagent was added to each well, with the exception of the blank well, and the plates were incubated at 37˚C for 60 min for antibody capture. Each well was then washed with diluted detergent five times. After washing, 50 $\mu$l chromogenic agent A and 50 $\mu$l chromogenic agent B were added to each well successively, and the plates were incubated at 37˚C for 15 min. Finally, 50 $\mu$l stop solution was added to each well to terminate the reaction, and the OD of each well was measured at a wavelength of 450 nm.

*Reverse transcription-quantitative PCR (RT-PCR)*. After routine digestion, HUVECs were cultivated in 6-well culture plates at a density of $1x10^5$ cells/well, and intervention was performed in accordance with the following groups: i) 1X PBS; ii) 100 pg/ml IL-6-EMPs; iii) 100 pg/ml lL-6-EMPs + 5 $\mu$M BCA; and iv) 100 pg/ml IL-6-EMPs + 10 $\mu$M BCA. After 24 h of intervention at 37˚C, total RNA was extracted using E.Z.N.A.® Total RNA Kit I and reverse transcribed into cDNA using RevertAid First Strand cDNA Synthesis Kit. The RT temperature protocol was according to manufacturer's protocol. The fluorophore used in qPCR was 2x SYBR Green PCR Mastermix. The thermocycling conditions were as follows: Initial denaturation at 95˚C for 5 min, followed by 40 cycles of denaturation (95˚C for 10 sec), annealing (60˚C for 15 sec) and 40 cycles of elongation (single fluorescence measurement at 72˚C for 15 sec), with a melting curve program of 60-95˚C, 0.11˚C/sec temperature rise (continuous fluorescence measurement), and cooling at 40˚C. Data were analyzed with the $2^{-\Delta\Delta Cq}$ method (25), using GAPDH as the normalization gene. The primers used in the present study are listed in Table I.

*Immunofluorescence (IF) staining*. After routine digestion, HUVECs were cultivated in 48-well culture plates at a density of $1x10^4$ cells/well. The intervention for group 1 was: i) 0 pg/ml IL-6-EMPs; and ii) 100 pg/ml IL-6-EMPs. The intervention for group 2 was: i) 1X PBS; ii) 100 pg/ml IL-6-EMPs; iii) 100 pg/ml IL-6-EMPs + 5 $\mu$M BCA; and iv) 100 pg/ml IL-6-EMPs + 10 $\mu$M BCA. After 24 h of intervention at 37˚C, the medium was discarded and the cells were washed three times with PBS. The cells were then fixed with 4% paraformaldehyde for 10 min at room temperature, washed with PBS three times and permeabilized for 5 min at room temperature with 0.1% Triton-X-100, which was then discarded. Subsequently, 3% BSA-PBS was added to the cells for 1 h at room temperature of blocking and was discarded. Washing was performed with 0.2% BSA-PBS three times. The primary antibodies of ICAM-1 (1:200) and ZO-1 (1:500) were then added into each well, respectively, and were incubated with the cells for 12 h at 4˚C in the dark. Subsequently, the primary antibodies were discarded, the cells were washed with 0.2% BSA-PBS three times, and the Fluor594-conjugated goat anti-rabbit IgG secondary antibody (1:500) was used to incubate the cells at room temperature for 2 h in the dark. After the secondary antibody was discarded, the cells were washed with 0.2% BSA-PBS three times, and were stained with DAPI reagent for 10 min at room temperature. Finally, the DAPI reagent was discarded, the cells were washed with 0.2% BSA-PBS three times, and an anti-fluorescence quenching agent was added. The cells were observed under a fluorescence microscope and images were captured.

*Western blot analysis*. After routine digestion, HUVECs were cultivated in 6-well culture plates at a density of $1x10^5$ cells/well. Group 1 was treated with: i) 1X PBS; ii) 0 pg/ml IL-6-EMPs; iii) 100 pg/ml IL-6-EMPs; and iv) 1,000 pg/ml IL-6-EMPs. Group 2 was treated with: i) 1X PBS; ii) 100 pg/ml IL-6-EMPs;

Table I. Primers for reverse transcription-quantitative PCR analysis.

| Gene | Forward primer (5'-3') | Reverse primer (5'-3') |
| --- | --- | --- |
| ICAM-1 | GTCACCTATGGCAACGACTCCTTC | AGTGTCTCCTGGCTCTGGTTCC |
| E-Selectin | GCACATCTCAGGGACAATGGACAG | CATCCTTCAGGACAGGCGAACTTG |
| GAPDH | GAAGGTCGGAGTCAACGGAT | CCTGGAAGATGGTGATGGG |

ICAM-1, intercellular cell adhesion molecule-1.

iii) 100 pg/ml IL-6-EMPs + 5 $\mu$M BCA; and iv) 100 pg/ml IL-6-EMPs + 10 $\mu$M BCA. After 24 h of intervention at 37°C, proteins were extracted from each group as following protocol: The supernatant was discarded and the cells were washed with PBS once. Subsequently, 116.4 $\mu$l RIPA buffer, 1.2 $\mu$l protease aprotinin, 1.2 $\mu$l protein phosphatase inhibitor and 1.2 $\mu$l PMSF were added to each well. After the culture plates were incubated on ice for 20 min, the lysis solution was collected in 1.5 ml EP tubes respectively. EP tubes were centrifuged at 4°C and 12,000 rpm for 20 min. The protein concentration of the supernatant was detected according to the instructions of the BCA protein assay kit. Then, the loading buffer was added into the EP tubes and they were incubated at 100°C for 15 min. The concentration of proteins was 20 $\mu$g per lane. Proteins were separated by SDS-PAGE on 8% gels and were subsequently transferred onto PVDF membranes. The membranes were washed with TBS-0.05%Tween (TBST) three times and blocked with 5% BSA-PBS with agitation for 1 h at room temperature. After blocking, the membranes were horizontally cut to probe proteins with different molecular weights, and incubated with different corresponding primary antibodies for 12-14 h at 4°C. The primary antibodies used included anti-β-actin (1:1,000), anti-ICAM (1:500), anti-ZO-1 (1:500), anti-NFκB (1:500), anti-IκB (1:500) and anti-VE-Cadherin (1:500). The membrane was then washed three times with 1X TBST and incubated with the corresponding horseradish peroxidase-labeled goat anti-rabbit IgG secondary antibodies (1:10,000) with agitation at room temperature for 1 h. Images of the membrane were acquired using West ECL and the Image Quant LAS 4000 system (Cytiva) and analyzed using ImageJ software V1.8.0 (National Institutes of Health).

*Animal model of femoral head necrosis.* Since Perthes disease is more likely to occur in male children, male Sprague-Dawley (SD) rats were selected for modeling. A total of 18 6-week-old male SD rats (weight, 194.0±9.068 g) were purchased from the Experimental Animal Center of Guangxi Medical University (Nanning, China). The animal experiment was approved by the Animal Care & Welfare Committee of Guangxi Medical University (approval no. 202111011; Nanning, China). The animal ethics review followed the guiding opinions on the treatment of laboratory animals (https://www.most.gov. cn/) issued by the Ministry of Science and Technology of the People's Republic of China and the guidelines for the ethical review of laboratory animal welfare issued by the National Standard GB/T35892-2018 of the People's Republic of China (26). All the animal experiments were carried out according to the ARRIVE guidelines (27).

The rats were reared at a room temperature of 25°C under 60% relative humidity and a 12-h light/dark cycle, with free access to water and food. The rats were randomly divided into the following three groups: The sham surgery group (n=6), the femoral head necrosis group (n=6) and the BCA group (drug group; n=6). The present study used the femoral neck girdling method, which is a common method of modeling femoral head necrosis in rats (6,28). The rats in the sham operation group underwent exposure of the femoral head through surgery without femoral neck girdling, whereas the femoral head necrosis group and the BCA group underwent femoral neck girdling. The surgery protocol was as follows: Following intraperitoneal injection of 200 mg/kg tribromoethanol for anesthesia and subcutaneous injection of 5 mg/kg carprofen for pain relief, the hip joint of the right lower limb was prepared and disinfected. The rats were fixed on the operating table in a prone position, deep anesthesia was ensured and the surgical area was disinfected with iodophor. The hip joint was checked to confirm that it was located under the gluteus and abductor muscles, to determine the position of the hip joint. Subsequently, an incision was made into the skin, the gluteus and abductor muscles were separated directly along the muscle fibers, and the hip capsule was exposed. The joint capsule was cut longitudinally along the femoral neck axis, and the hip joint was pulled and bent longitudinally, causing the femoral head to be semi-dislocated, thus exposing the round ligament, which was cut off. Two No. 1-sized non-absorbable sutures were placed around the femoral neck and tightly crossed to block the ascending branch of the circumflex femoral artery supplying the epiphysis of the femoral head. Finally, the joint capsule and gluteal muscle were repaired in turn, and the skin was closed in layers (28,29).

After modeling, the rats were observed every day, paying particular attention to fur color, wound sutures, wound healing, any hunched-back behavior and food and drink intake, to monitor the health of the animals. A total of 2 days after surgery, each rat received intramuscular injection of 18 mg/kg penicillin daily to prevent infection. In addition, the BCA group was injected with BCA (2.5 mg/kg) intraperitoneally every 2 days for 4 weeks, whereas the sham operation group and the femoral head necrosis group were injected with 1X PBS every 2 days at the same dose as the BCA group for 4 weeks. In the present study, excessive fur grooming, hunched behavior and 20% body weight loss were used as evaluation indexes of humane endpoints. When the three abnormal behaviors occurred at the same time, the humane endpoint was considered to be reached. The weight of the rats in the sham group, femoral head necrosis group and BCA group at

the beginning of the study was 195.8±7.627, 192.7±7.992 and 193.5±12.29 g respectively; the weight of the rats in the sham group, femoral head necrosis group and BCA group at the end of the study was 278.7±10.25, 276.8±5.776 and 280.7±13.16 g, respectively. No rats reached the humane endpoint before the end of the study (30,31). After 4 weeks, referring to the animal euthanasia methods recommended by the AVMA Guidelines for the Euthanasia of Animals (https://www.avma.org/), excessive anesthesia with pentobarbital sodium (200 mg/kg; intraperitoneal injection) was used to euthanize the animals. The death of the rats was confirmed as follows: By verifying a lack of respiration or pulse; confirmation of a lack of heartbeat for >5 min, as determined using a stethoscope or by touching the chest cavity; disappearance of the corneal and nerve reflexes; and pupil dilation.

After euthanasia, the femurs were removed and fixed with 4% paraformaldehyde for 48 h at room temperature. After fixation, 10% ethylenediaminetetraacetic acid was utilized to decalcify the fixed rat femoral head specimens for 3 weeks at 25-30˚C. Subsequently, the specimens were embedded in paraffin and sectioned with a thickness of 4 $\mu$m, and the sections were processed for IL-6 immunohistochemical staining. Firstly, the sections were immersed in fresh xylene for 10 min for three times. The sections were subsequently soaked in gradient ethanol: 100% for 3 min for three times, 95% for 3 min for two times, 75% for 3 min for two times. The sections were washed with sterilized pure water for 1 min for three times. Then, the sections were immersed in the sodium citrate buffer and heated in the microwave until the buffer boiled, and the microwave was immediately maintained at low heat for 10 min. After that, the sections were removed from the microwave and cooled naturally to room temperature. We washed the sections with PBS for 3 min for three times and added an appropriate amount of endogenous peroxidase blocker from the Universal two-step detection kit and incubated at room temperature for 10 min. An appropriate amount of IL-6 primary antibody (1:100) was added to the sections, and they were placed in a wet box and incubated at 4˚C overnight. At the end of the incubation, the sections were washed with PBS for 3 min for three times. An appropriate amount of reaction enhancing solution from the Universal two-step detection kit was added to the sections, which were incubated at 37˚C for 20 min. After incubation, the sections were washed with PBS for 3 min for three times. An appropriate amount of enhanced enzyme-linked sheep anti mouse/rabbit IgG polymer from the Universal two-step detection kit was added to the sections and the sections were incubated at 37˚C for 20 min. An appropriate amount of DAB colorimetric solution was added to the sections and the sections were incubated for 5-8 min at room temperature. And the sections were washed with tap-water to terminate staining. Finally, the sections were dyed with hematoxylin solution for 3-5 min at room temperature and washed with tap-water to terminate staining. The sections were observed under microscope (BX53F; Olympus Corporation) and images were captured. ImageJ Software V1.8.0 (National Institutes of Health) was used to count the number of IL-6-positive cells. In addition, rat liver and kidney samples were collected. To observe the hepatorenal toxicity of BCA, hematoxylin and eosin (H&E) staining

was performed as the following protocol: The specimens were embedded in paraffin and sectioned with a thickness of 3 $\mu$m. After dewaxing, hydration and pretreatment, the sections were dyed with hematoxylin solution for 3-5 min at room temperature and with eosin solution for 15 sec at room temperature. After staining, all sections were observed under a microscope (BX53F; Olympus Corporation) and images were captured.

*Statistical analysis.* All the experiments were repeated at least three times. All data analyses were carried out using SPSS 26.0 (IBM Corp.) and presented as mean ± standard deviation. The charts were generated using GraphPad 7.0 (Dotmatics) and grouped in Adobe Illustrator 2019 (Adobe Systems, Inc.). Differences between two groups were analyzed using unpaired Student's t-test. Differences between three or more groups were analyzed using one-way ANOVA followed by Tukey's post hoc test. P<0.05 was considered to indicate a statistically significant difference.

## Results

*EMPs secreted by IL-6-stimulated HUVECs can induce endothelial dysfunction.* HUVECs were treated with different concentrations of IL-6 (0, 1, 10, 100 and 1,000 pg/ml) to obtain IL-6-EMPs. The endocytosis experiment revealed that IL-6-EMPs were absorbed into HUVECs and played a role in affecting the function of HUVECs (Fig. 1A). In addition, ELISAs were performed to explore the effect of IL-6-EMPs on the markers of endothelial cell dysfunction. The results showed that treatment with 100 pg/ml IL-6-EMPs promoted the expression of VCAM-1 and ICAM-1 in HUVECs compared with the PBS group; however, they did not affect the expression of E-Selectin (Fig. 1B). Notably, peak ICAM-1 levels were detected following treatment with 100 pg/ml IL-6-EMPs. By contrast, 1,000 pg/ml IL-6-EMPs inhibited the levels of ICAM-1 and VCAM-1 compared with the 100 pg/ml IL-6-EMPs group. It has been demonstrated that damaged endothelial cells can promote monocyte adhesion (32). After the HUVECs were treated with different concentrations of IL-6-EMPs (0, 1, 10, 100 and 1,000 pg/ml), they were co-cultured with fluorescent-labeled monocytes. The results showed that IL-6-EMPs can promote monocyte adhesion to HUVECs in a concentration-dependent manner within the concentration range of 0-100 pg/ml IL-6 (Fig. 1C). Similar to the ELISA results, monocyte adhesion was also inhibited by 1,000 pg/ml IL-6-EMPs compared with the 100 pg/ml IL-6-EMPs group. In addition, IF-staining suggested that IL-6-EMPs reduced the expression of ZO-1, but promoted the expression of ICAM-1 in HUVECs, indicating that 100 pg/ml IL-6-EMPs could induce endothelial dysfunction (Fig. 1D and E).

*BCA can inhibit IL-6-EMP-induced endothelial dysfunction.* BCA is an isoflavone and its chemical structure is shown in Fig. 2A. HUVECs were treated with different concentrations of BCA (0, 2.5, 5, 10, 20 and 40 $\mu$M) and IL-6-EMPs (0, 1, 10, 100 and 1,000 pg/ml) to determine whether BCA and IL-6-EMPs had toxic effects on HUVECs. The results of the CCK8 assay showed that 0-20 $\mu$M BCA and IL-6-EMPs did
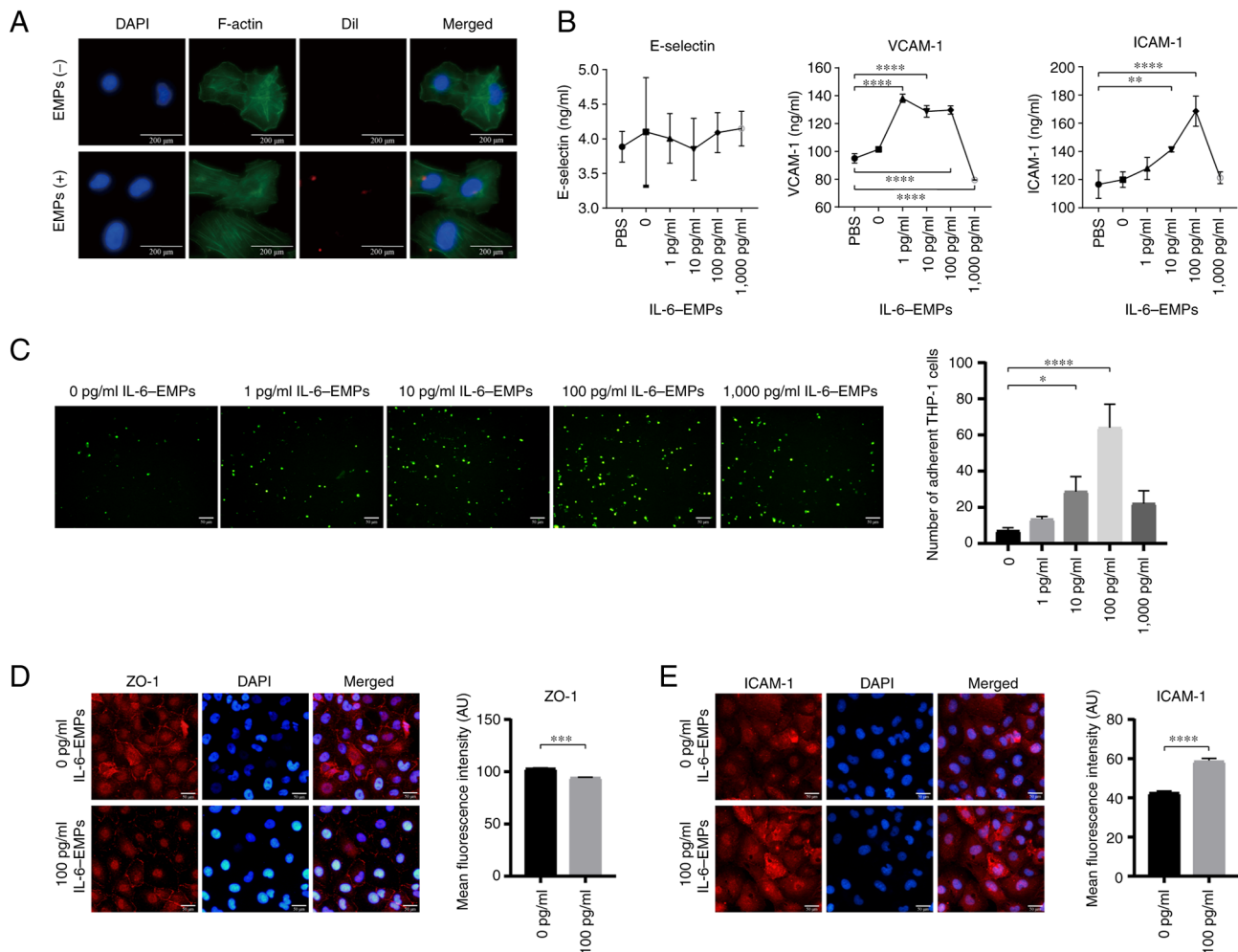
Figure 1. EMPs stimulated by IL-6 induce endothelial dysfunction. (A) EMPs labeled with red fluorescent Dil were endocytosed by HUVECs. Scale bar=200 $\mu$m. (B) EMPs stimulated by 100 pg/ml IL-6 significantly promoted the levels of ICAM-1 and VCAM-1 in HUVECs but did not affect the levels of E-Selectin. (C) Monocyte adhesion is increased after endothelial cell injury. The endothelial-monocyte adhesion assay showed that IL-6 promoted monocyte adhesion to HUVECs in a concentration-dependent manner in the concentration range of 0-100 pg/ml IL-6. Green fluorescence represents monocytes. Scale bar=50 $\mu$m. (D) EMPs stimulated by 100 pg/ml IL-6 decreased the expression of ZO-1 (n=3). Scale bar=50 $\mu$m. (E) EMPs stimulated by 100 pg/ml IL-6 promoted the expression of ICAM-1 and promoted endothelial dysfunction (n=3). Scale bar=50 $\mu$m. *P<0.05, **P<0.01, ***P<0.001, ****P<0.0001. EMPs, endothelial microparticles; HUVECs, human umbilical vein endothelial cells; ICAM-1, intercellular cell adhesion molecule-1; VCAM-1, vascular cell adhesion molecule-1; ZO-1, zonula occludens-1.

not affect the viability of HUVECs; however, co-treatment with 100 pg/ml IL-6-EMPs and 20 or 40 $\mu$M BCA reduced the viability of HUVECs compared with the control group (Fig. 2B). Furthermore, based on the results of ELISA (Fig. 1B), adhesion experiment (Fig. 1C) and CCK8, HUVECs were treated with 100 pg/ml IL-6-EMPs and 0, 5 and 10 $\mu$M BCA, and RT-qPCR, adhesion assay and IF staining were performed. RT-qPCR results revealed that BCA could reduce the expression levels of ICAM-1 and E-selectin in HUVECs in a concentration-dependent manner compared with the increase induced by 100 pg/ml IL-6-EMPs (Fig. 2C). The results of the adhesion assay demonstrated that BCA could inhibit IL-6-EMPs-induced endothelial dysfunction in a concentration-dependent manner, thereby reducing the number of adherent monocytes (Fig. 2D). Furthermore, IF staining results revealed that BCA increased the expression of ZO-1 compared with the increase induced by 100 pg/ml IL-6-EMPs, and thus inhibited the endothelial dysfunction induced by IL-6-EMPs (Fig. 2E).

*BCA inhibits endothelial dysfunction induced by IL-6-EMPs via the NFκB signaling pathway.* Western blot analysis was performed to investigate the activation of the NFκB signaling pathway and the mechanism underlying the inhibitory effect of BCA on IL-6-EMPs-induced endothelial dysfunction. Following treatment of HUVECs with 100 and 1,000 pg/ml IL-6-EMPs, the expression levels of ICAM-1 were elevated and those of ZO-1 were decreased, indicating that IL-6-EMPs induced endothelial dysfunction (Fig. 3A and B). Subsequently, HUVECs were treated with 100 pg/ml IL-6-EMPs combined with 0, 5 and 10 $\mu$M BCA. The results showed that BCA could reduce the expression levels of NFκB in a dose-dependent manner, while increasing the expression levels of IκB compared with the changes induced by 100 pg/ml IL-6-EMPs (Fig. 3C and D). Moreover, after intervention with BCA, the protein expression levels of the endothelial dysfunction marker ICAM-1 was decreased, whereas those of ZO-1 and VE-cadherin were increased compared with the changes induced by 100 pg/ml IL-6-EMPs.
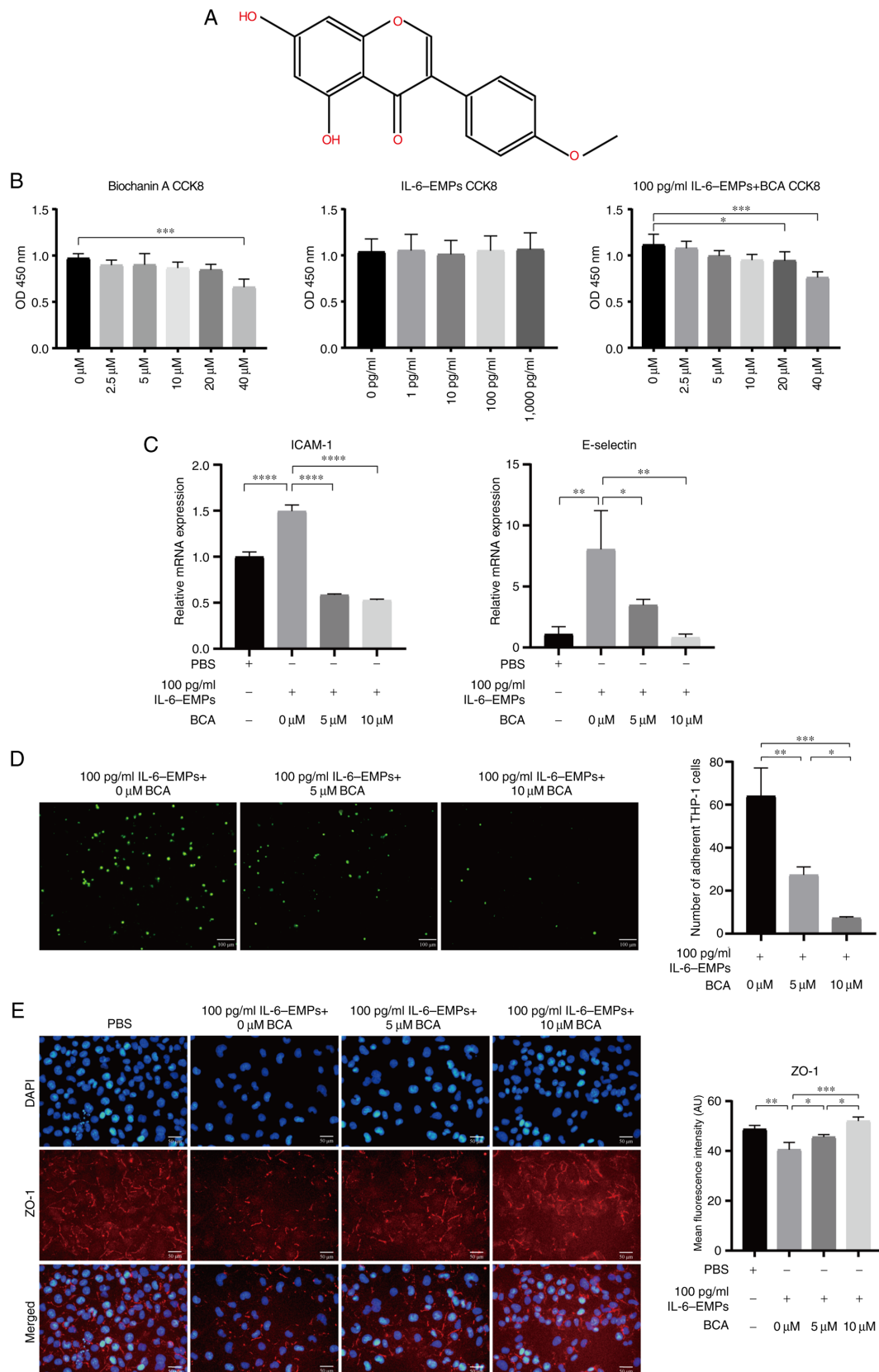
Figure 2. BCA inhibits endothelial dysfunction induced by IL-6-EMPs in the non-cytotoxic concentration range. (A) Chemical structure of BCA. (B) CCK8 assay results showed that BCA had no toxic effect on cells in the concentration range of 0-20 $\mu$M, IL-6-EMPs had no toxic effect on cells in the concentration range of 0-1,000 pg/ml, and 100 pg/ml IL-6-EMPs + 0-10 $\mu$M BCA had no toxic effect on cells (n=3). (C) After treatment with BCA, the indexes of endothelial dysfunction ICAM-1 and E-selectin were decreased with the increase in BCA concentration, indicating that BCA can effectively reduce the endothelial dysfunction induced by IL-6-EMPs (n=3). (D) Adhesion assay showed that BCA could inhibit the injury of endothelial cells induced by IL-6-EMPs and reduce the adhesion of monocytes to human umbilical vein endothelial cells. Green fluorescence represents monocytes (n=3). Scale bar=100 $\mu$m. (E) IL-6-EMPs (100 pg/ml) decreased the expression of ZO-1. After treatment with BCA, the endothelial dysfunction induced by IL-6-EMPs was inhibited and the expression of ZO-1 was increased (n=3). Scale bar=50 $\mu$m. *P<0.05, **P<0.01, ***P<0.001, ****P<0.0001. BCA, biochanin A; CCK8, Cell Counting Kit 8; EMPs, endothelial microparticles; ICAM-1, intercellular cell adhesion molecule-1; ZO-1, zonula occludens-1.
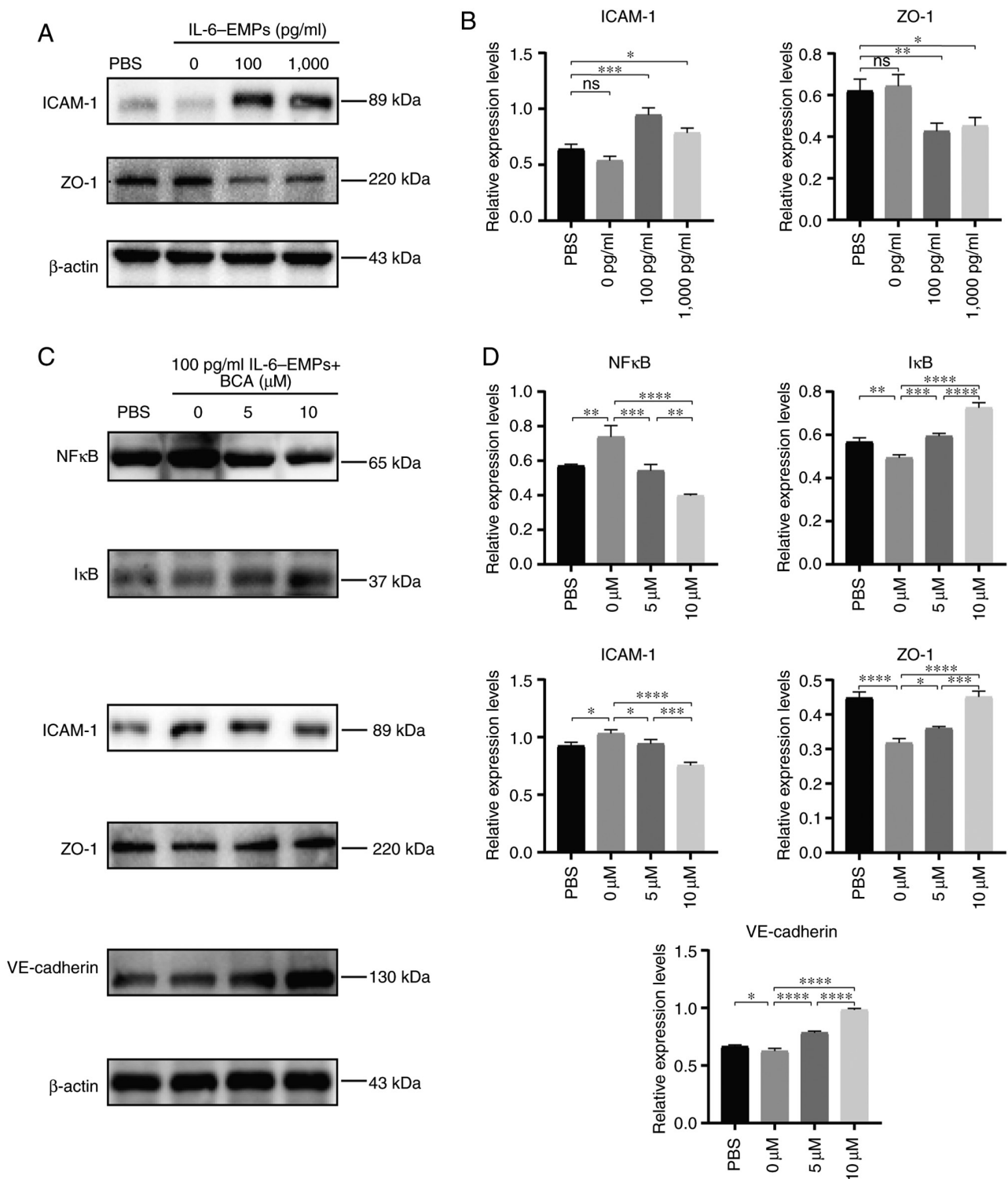
Figure 3. BCA inhibits endothelial dysfunction via the NFκB signaling pathway. (A) After HUVECs were treated with different concentrations of IL-6-EMPs (0, 100 and 1,000 pg/ml), the expression levels of ICAM-1 and ZO-1 were analyzed by western blotting. Representative images showed that the expression levels of ICAM-1 were increased with the increase in IL-6-EMPs concentration, whereas the expression levels of ZO-1 were decreased with the increase in IL-6-EMPs concentration (n=3). (B) Relative expression levels of ICAM-1 and ZO-1 were calculated. (C) HUVECs were treated with 100 pg/ml IL-6-EMPs + BCA (0, 5 and 10 $\mu$M). After treatment, the expression levels of NFκB, IκB, ICAM-1, ZO-1 and VE-cadherin were analyzed by western blotting. Representative images showed that the expression levels of NFκB and ICAM-1 were decreased with the increase in BCA concentration, and the expression levels of IκB, ZO-1 and VE-cadherin were increased with the increase in BCA concentration (n=3). (D) Relative expression levels of NFκB, IκB, ICAM-1, ZO-1 and VE-cadherin were calculated. *P<0.05, **P<0.01, ***P<0.001, ****P<0.0001. BCA, biochanin A; EMPs, endothelial microparticles; HUVECs, human umbilical vein endothelial cells; ICAM-1, intercellular cell adhesion molecule-1; ns, not significant; ZO-1, zonula occludens-1.

*BCA inhibits the expression of IL-6 in bone tissues after ischemic necrosis of the femoral head*. A rat model of ischemic necrosis of the femoral head was established to investigate

the effect of BCA on the expression levels of IL-6 in bone tissues. The femoral head in the sham surgery group remained intact, whereas that in the femoral head necrotic group
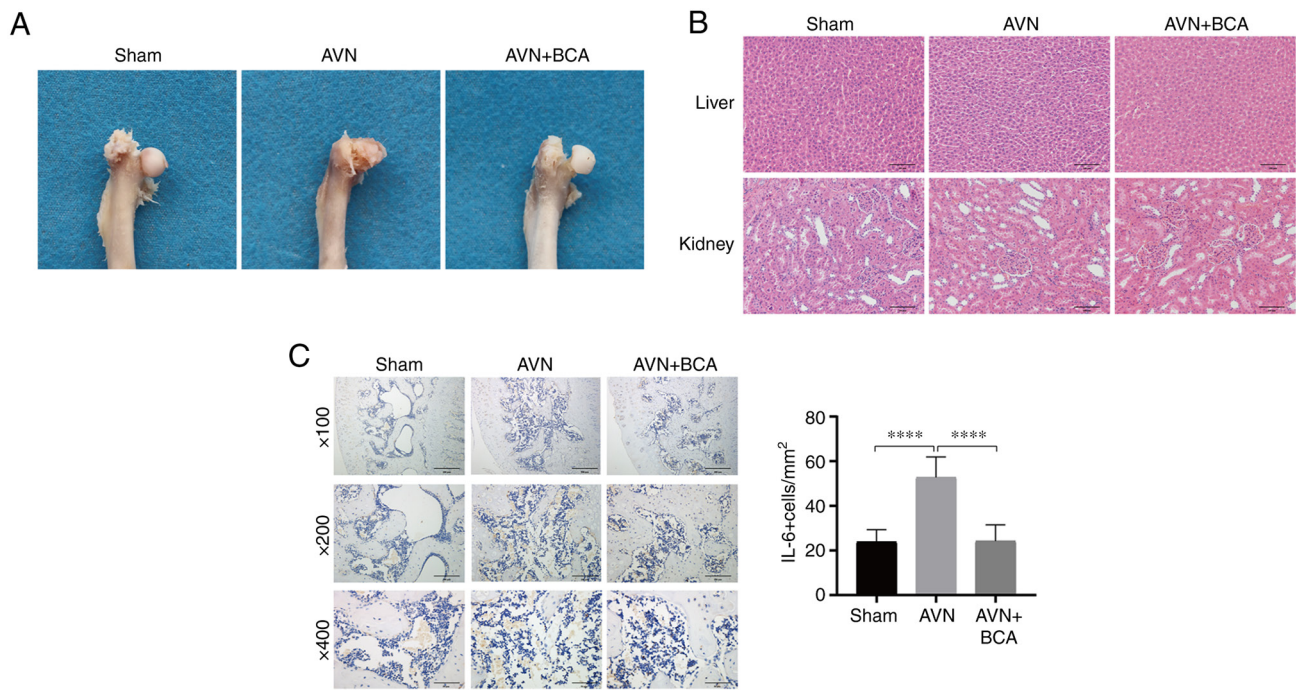
Figure 4. BCA inhibits endothelial dysfunction and alleviates deformation of the femoral head in *in vivo* experiments. (A) Macroscopic images showed that the femoral head in the sham operation group was in good shape, whereas an obvious collapse and deformity of the femoral head was observed in the femoral head necrosis group, which were reduced in the BCA group (n=6). (B) Hematoxylin and eosin staining sections showed no marked histological differences in the liver and kidney of the three groups of rats (n=6). Scale bar=100 $\mu$m. (C) Immunohistochemistry and statistical analysis of pathological sections of the femoral head showed that the expression levels of IL-6 were decreased after treatment with BCA (n=6). Scale bar=200, 100, 50 $\mu$m for 'x100', 'x200', 'x400', respectively. $^{****}$P<0.0001. BCA, biochanin A. AVN, avascular necrosis.

collapsed and appeared flatter and more severely damaged than that in the BCA group (Fig. 4A). H&E staining of liver and kidney sections indicated that there was no marked difference in histology between the three groups (Fig. 4B). Immunohistochemical analysis suggested that the expression levels of IL-6 were significantly elevated in the femoral head section of the femoral head necrotic group compared with those in the other two groups, indicating that BCA could reduce the expression of IL-6 after the ischemic necrosis of the femoral head (Fig. 4C). Based on the aforementioned *in vitro* and *in vivo* experiments, the present study concluded that BCA could reduce the expression levels of ICAM-1 and E-selectin, and improve endothelial dysfunction induced by IL-6-EMPs through the NF$\kappa$B pathway, thus improving the collapse of femoral head in femoral head necrosis rats. The potential mechanism underlying the effects of BCA in the treatment of Perthes disease is shown in Fig. 5.

**Discussion**

Perthes disease is a disabling and teratogenic disease in children, which is characterized by ischemic necrosis of the femoral head and may cause the deformation of femoral head if the diagnosis and treatment are not timely. In the absence of any intervention, the collapse and deformation of the femoral head can induce premature arthritis, which eventually causes different degrees of disability in children (33). At present, the clinical treatment of Perthes disease includes absolute weight-free bed rest (avoiding trying to stand with affected lower limb) and surgical treatment (34). However,
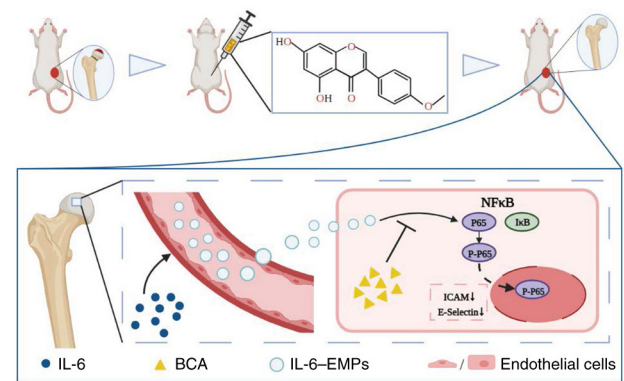


Figure 5. Mechanism underlying the effects of BCA on the treatment of Perthes disease. BCA inhibits endothelial dysfunction induced by IL-6-EMPs via the NF$\kappa$B pathway, and may therefore be considered a potential drug for the treatment of Perthes disease. Created with BioRender.com. BCA, biochanin A; EMPs, endothelial microparticles; ICAM, intercellular cell adhesion molecule; p, phosphorylated.

these treatments are not very efficient, and no effective drug treatment exists. Therefore, it is necessary to study the etiology, pathogenesis and possible therapeutic drugs for Perthes disease. Our previous study (12) found that in patients with Perthes disease, upregulation of IL-6 stimulated EMPs to induce endothelial dysfunction. And the same result was found in a rat model of ischemic necrosis of the femoral head in the present study. Moreover, BCA could inhibit IL-6-EMPs-induced endothelial dysfunction through

the NFκB signaling pathway, and may thus be considered a potential drug for Perthes disease.

The etiology of Perthes disease has not been clarified, and numerous hypotheses have been proposed for its pathogenesis. The hypothesized pathogenic factors include microtrauma, tobacco exposure, prenatal factors, blood hypercoagulation status and collagen mutations (1). However, these assumptions have not been fully confirmed or are controversial. Notably, it has been shown that endothelial dysfunction induced by IL-6-EMPs may be a key pathological process in Perthes disease (7). Kuroyanagi *et al* (35) established an animal model of Perthes disease and found that IL-6 is significantly increased in the joint fluid after induction of ischemic necrosis of the femoral head. In addition, IL-6 gene knockout can result in revascularization in a mouse model of Perthes disease (35). Our previous study (12) demonstrated that the expression levels of IL-6 are elevated in the plasma of patients with Perthes disease and that IL-6 is associated with CD31+/CD42b- EMPs. EMPs are exosomes with a diameter of 100-1,000 nm, which are secreted into the plasma after endothelial cell dysfunction (36), and this was characterized by flow cytometry in our previous study (12). The antigen carried on the EMP surface is the same as that found in endothelial cells; therefore, the state of endothelial cells can be assessed by detecting the cell-surface antigen of EMPs (37). The expression of CD31 is elevated during endothelial apoptosis, and the expression of CD62E is increased upon endothelial cell activation; therefore, the ratio of CD31+CD42b-/CD62E+ is commonly used to assess the extent of endothelial dysfunction (38). In our previous study (12), it was revealed that the proportion of CD62E+ EMPs are not significantly elevated compared with the control group, but the ratio and proportion of CD31+CD42b- EMPs to CD62E+ EMPs was higher in patients with Perthes disease compared with the control group. This phenomenon suggested that the number of apoptotic EMPs may be greater than that of activated EMPs in patients with Perthes disease. These results from our previous study (12) indicated that IL-6 may be the key inflammatory factor for the induction of endothelial dysfunction in Perthes disease and that IL-6-EMPs-induced endothelial dysfunction could be the key to the treatment of Perthes disease.

Endothelial cells contain several characteristic markers, such as VCAM-1, E-selectin, von Willebrand factor, ICAM-1 and endothelial nitric oxide synthase (NOS), which can be utilized as indicators of endothelial dysfunction. ICAM-1 is a surface glycoprotein and adhesion receptor that is involved in various physiological processes, such as leukocyte adhesion (39), tumor cell transfer (40), barrier function (41), proliferation (42) and epithelial cell activation (43). It is poorly expressed in endothelial, immune and epithelial cells, but is upregulated when stimulated by inflammation (44). VCAM-1 is an adhesion factor that mediates the binding of eosinophils, monocytes and other vascular endothelial cells. It is mostly expressed in smooth muscle and vascular endothelial cells, and serves a role in endothelial dysfunction by participating in the development and progression of inflammation; reducing VCAM-1 gene expression can alleviate vascular inflammation and endothelial dysfunction (45-47). In Perthes disease, upregulation of the inflammatory factor IL-6 increases the expression levels of VCAM-1 and ICAM-1 in endothelial

cells, and impairs the permeability of endothelial cells, which subsequently promotes endothelial dysfunction (48). ZO-1 has a marked effect on the maintenance of the blood-brain barrier and the close connection between endothelial cells (48). It is also an important protein in the physiological process of angiogenesis. The reduction in ZO-1 expression decreases the tight connection of endothelial cells and increases their permeability. In the present study, treating endothelial cells with IL-6-EMPs promoted monocyte adhesion to HUVECs in a dose-dependent manner, and significantly increased VCAM-1 and ICAM-1 production. IF analysis also revealed that the expression levels of ZO-1 were decreased, whereas those of ICAM-1 were increased in endothelial cells. Therefore, it was indicated that IL-6-EMPs induced endothelial dysfunction.

At present, no effective clinical drug exists for Perthes disease. Certain researchers have attempted to use antiosteoporosis drugs, such as bisphosphate and strontium ranelate (4,5), to treat this disease. However, bisphosphate may lead to side effects, such as jaw necrosis, atypical femoral fractures and delayed bone healing in children with osteogenesis imperfecta (49-51). And strontium ranelate may have undesirable side effects including allergy and increased risk for cardiovascular events in systemic use (52). These side effects and adverse reactions limit the clinical application of these two drugs. Therefore, the active exploration of effective clinical drugs for Perthes disease is of great importance. BCA can be extracted from plants, such as Caulis Spatholobi (13), soybean, peanut, red clover, chickpea and alfalfa (14). Among its various biological characteristics, its anti-inflammatory effects have attracted attention. It has been shown that the anti-inflammatory characteristics of BCA are mainly manifested by inhibiting the expression of VCAM-1, IL-8, ICAM-1 and tumor necrosis factor α (TNF-α) in HUVECs, thereby reducing the activation of NFκB (53). Furthermore, BCA blocks the expression of NFκB in macrophages to reduce the lipopolysaccharide-activated expression of NO and inducible NOS (24), and can also effectively inhibit the expression of TNF-α and IL-6. Our previous study found that BCA can inhibit bone resorption and osteoclast production via the MAPK and NFκB signaling pathways (23). The role of BCA in animals has also been reported. BCA can inhibit the phosphorylation level of prostaglandin E-2, NOS-2, NFκB and cyclooxygenase-2 to protect rat chondrocytes from IL-induced inflammation (54). Notably, there are other Chinese traditional medicine extracts or prescriptions that can resist inflammation and improve endothelial dysfunction, such as hederagenin (55), cycloastragenol (56), epigallocatechin-3-gallate (57), He xue ming mu tablet (58), glycyrrhizic acid (59), tanshinone IIA sodium sulfonate (60) and quercetin (61), but some of them exhibit clinical toxicity and side effects, such as nausea, insomnia and hepatotoxicity. At present, there is no relevant research comparing BCA with the aforementioned drugs in terms of anti-inflammatory activity and improving endothelial dysfunction, therefore it is not possible to identify a clear advantage of BCA over the aforementioned drugs. However, in the present animal experiments, it was revealed that BCA had no obvious hepatorenal toxicity through H&E staining of the liver and kidney specimens of the three groups of rats, suggesting that BCA may exhibit low toxicity. Therefore, the present study speculated on whether BCA could inhibit IL-6-EMPs-induced endothelial dysfunction via the NFκB pathway. It was revealed

that the expression levels of ICAM-1 were decreased after intervention with IL-6-EMPs and different concentrations of BCA. The outcomes of IF staining demonstrated that the expression of ZO-1 was increased by BCA, and western blotting showed that the expression levels of NFκB were decreased after BCA intervention compared with those before BCA intervention, whereas the expression of IκB was increased. These findings indicated that BCA may inhibit endothelial dysfunction induced by IL-6-EMPs via the NFκB pathway.

In young animal models, Perthes disease may be induced through the ischemic osteonecrosis of the femoral head by ligation of the femoral neck. Yamaguchi *et al* (62) showed that in piglets, a model of ischemic osteonecrosis of the femoral head can be constructed by ligating the femoral neck, cutting off the round ligament, and implementing supra knee amputation at the junction of the distal epiphysis and epiphysis of the femur. In this model, the IL-6 receptor monoclonal antibody can reduce hip synovitis and osteoclast bone resorption, and increase bone formation. In addition, a mouse model of bone ischemic necrosis can be successfully induced through the microscopic burning of four blood vessels, including the popliteal artery branch at the distal end of the femur and the medial, central and lateral blood vessels of the knee (35,63). In the present study, a rat model of ischemic necrosis of the femoral head was established in consideration of the fact that we were unable to raise piglets and complete the femoral head necrosis model with piglets and mice under the conditions provided by our experimental animal center in a short term. After successful modeling, the femoral heads in the sham operation group were smooth and complete; those in the femoral head necrosis group were flattened, collapsed and severely damaged; and those in the BCA group were less damaged than those in the femoral head necrosis group and showed improvements in deformities. The results of the present *in vivo* study suggested that BCA could alleviate deformation of the femoral head in Perthes disease. In addition, the immunohistochemical staining of pathological sections revealed that BCA reduced the expression levels of IL-6 in femoral head tissue, indicating that BCA may reduce the secretion of IL-6-EMP and inhibit the endothelial dysfunction induced by IL-6-EMPs *in vivo*. In conclusion, BCA can effectively inhibit endothelial dysfunction in Perthes disease and improve deformation of the femoral head. Therefore, it may be considered as a potential drug for the treatment of Perthes disease.

In Perthes disease, IL-6-EMPs can induce endothelial dysfunction; however, via the NFκB pathway, BCA can inhibit IL-6-EMPs-induced endothelial dysfunction and reduce the expression levels of IL-6 in bone tissue following ischemic necrosis of the femoral head. These findings suggested that BCA may be utilized as a therapeutic drug for Perthes disease.

## Acknowledgements

## Availability of data and materials

The datasets generated and/or analyzed during the current study are available from the corresponding author on reasonable request.

## Authors' contributions

XD and SL confirm the authenticity of all the raw data. XD and SL were involved in conceptualization and design of the methodology. JL and CL performed the experiments. ST, XL, RL and YL contributed to data curation. BL, QH and XC analyzed the data. JL wrote the original draft. SL, CL, RL and YL reviewed and edited the manuscript. All authors read and approved the final manuscript.

## Ethics approval and consent to participate

The animal experiment was approved by the Animal Care & Welfare Committee of Guangxi Medical University (approval no. 202111011; Nanning, China).

## Patient consent for publication

Not applicable.

## Competing interests

The authors declare that they have no competing interests.

## References

1. Leroux J, Abu Amara S and Lechevallier J: Legg-Calvé-Perthes disease. Orthop Traumatol Surg Res 104: S107-S112, 2018.
2. Zhao Y, Liao S, Lu R, Dang H, Zhao J and Ding X: Endothelial nitric oxide synthase gene polymorphism is associated with Legg-Calvé-Perthes disease. Exp Ther Med 11: 1913-1917, 2016.
3. Kim S, Oh H, Lim J, Cho S and Jung S: Results of early proximal femoral osteotomy at skeletal maturity in Legg-Calvé-Perthes disease: Implication for the bypass of fragmentation stage. J Pediatr Orthop 41: e768-e773, 2021.
4. Little D, McDonald M, Sharpe I, Peat R, Williams P and McEvoy T: Zoledronic acid improves femoral head sphericity in a rat model of perthes disease. J Orthop Res 23: 862-868, 2005.
5. Kim HKW, Randall TS, Bian H, Jenkins J, Garces A and Bauss F: Ibandronate for prevention of femoral head deformity after ischemic necrosis of the capital femoral epiphysis in immature pigs. J Bone Joint Surg Am 87: 550-557, 2005.
6. Johnson CP, Wang L, Tóth F, Aruwajoye O, Kirkham B, Carlson CS, Kim HKW and Ellermann JM: Quantitative susceptibility mapping detects neovascularization of the epiphyseal cartilage after ischemic injury in a piglet model of Legg-Calvé-Perthes disease. J Magn Reson Imaging 50: 106-113, 2019.
7. Perry DC, Green DJ, Bruce CE, Pope D, Dangerfield P, Platt MJ, Hall AJ and Jones H: Abnormalities of vascular structure and function in children with Perthes disease. Pediatrics 130: e126-e131, 2012.

8. Kamiya N, Yamaguchi R, Adapala N, Chen E, Neal D, Jack O, Thoveson A, Gudmundsson P, Brabham C, Aruwajoye O, *et al*: Legg-Calvé-Perthes disease produces chronic hip synovitis and elevation of interleukin-6 in the synovial fluid. J Bone Miner Res 30: 1009-1013, 2015.

9. Kamiya N, Kuroyanagi G, Aruwajoye O and Kim HKW: IL6 receptor blockade preserves articular cartilage and increases bone volume following ischemic osteonecrosis in immature mice. Osteoarthritis Cartilage 27: 326-335, 2019.

10. Kao CY and Papoutsakis ET: Extracellular vesicles: Exosomes, microparticles, their parts, and their targets to enable their biomanufacturing and clinical applications. Curr Opin Biotechnol 60: 89-98, 2019.

11. Deng F, Wang S and Zhang L: Endothelial microparticles act as novel diagnostic and therapeutic biomarkers of circulatory hypoxia-related diseases: A literature review. J Cell Mol Med 21: 1698-1710, 2017.

12. Li B, Huang Q, Lin C, Lu R, Wang T, Chen X, Liu Z, Liu Y, Wu J, Wu Y, *et al*: Increased circulating CD31+/CD42b-EMPs in Perthes disease and inhibit HUVECs angiogenesis via endothelial dysfunction. Life Sci 265: 118749, 2021.

13. Liu XY, Zhang YB, Yang XW, Xu W, Liu L, Zhang P, Gong Y, Liu NF and Peng KF: Simultaneous determination of twenty-five compounds with anti-inflammatory activity in Spatholobi Caulis by using an optimized UFLC-MS/MS method: An application to pharmacokinetic study. J Pharm Biomed Anal 204: 114267, 2021.

14. Sarfraz A, Javeed M, Shah M, Hussain G, Shafiq N, Sarfraz I, Riaz A, Sadiqa A, Zara R, Zafar S, *et al*: Biochanin A: A novel bioactive multifunctional compound from nature. Sci Total Environ 722: 137907, 2020.

15. Hsu YN, Shyu HW, Hu TW, Yeh JP, Lin YW, Lee LY, Yeh YT, Dai HY, Perng DS, Su SH, *et al*: Anti-proliferative activity of biochanin A in human osteosarcoma cells via mitochondrial-involved apoptosis. Food Chem Toxicol 112: 194-204, 2018.

16. Yu C, Zhang P, Lou L and Wang Y: Perspectives regarding the role of biochanin A in humans. Front Pharmacol 10: 793, 2019.

17. Khanna S, Stewart R, Gnyawali S, Harris H, Balch M, Spieldenner J, Sen CK and Rink C: Phytoestrogen isoflavone intervention to engage the neuroprotective effect of glutamate oxaloacetate transaminase against stroke. FASEB J 31: 4533-4544, 2017.

18. Liang F, Cao W, Huang Y, Fang Y, Cheng Y, Pan S and Xu X: Isoflavone biochanin A, a novel nuclear factor erythroid 2-related factor 2 (Nrf2)-antioxidant response element activator, protects against oxidative damage in HepG2 cells. Biofactors 45: 563-574, 2019.

19. Hanski L, Genina N, Uvell H, Malinovskaja K, Gylfe Å, Laaksonen T, Kolakovic R, Mäkilä E, Salonen J, Hirvonen J, *et al*: Inhibitory activity of the isoflavone biochanin A on intracellular bacteria of genus Chlamydia and initial development of a buccal formulation. PLoS One 9: e115115, 2014.

20. Jalaludeen AM, Ha WT, Lee R, Kim JH, Do JT, Park C, Heo YT, Lee WY and Song H: Biochanin A ameliorates arsenic-induced hepato- and hematotoxicity in rats. Molecules 21: 69, 2016.

21. Sangeethadevi G, V V SU, Jansy Isabella RAR, Saravanan G, Ponmurugan P, Chandrasekaran P, Sengottuvelu S and Vadivukkarasi S: Attenuation of lipid metabolic abnormalities, proinflammatory cytokines, and matrix metalloproteinase expression by biochanin-A in isoproterenol-induced myocardial infarction in rats. Drug Chem Toxicol 45: 1951-1962, 2022.

22. Xue Z, Li A, Zhang X, Yu W, Wang J, Li Y, Chen K, Wang Z and Kou X: Amelioration of $PM_{2.5}$-induced lung toxicity in rats by nutritional supplementation with biochanin A. Ecotoxicol Environ Saf 202: 110878, 2020.

23. Liao S, Feng W, Liu Y, Wang Z, Ding X, Song F, Lin X, Song H, Kc A, Su Y, *et al*: Inhibitory effects of biochanin A on titanium particle-induced osteoclast activation and inflammatory bone resorption via NF-κB and MAPK pathways. J Cell Physiol 236: 1432-1444, 2021.

24. Kole L, Giri B, Manna SK, Pal B and Ghosh S: Biochanin-A, an isoflavon, showed anti-proliferative and anti-inflammatory activities through the inhibition of iNOS expression, p38-MAPK and ATF-2 phosphorylation and blocking NFκB nuclear translocation. Eur J Pharmacol 653: 8-15, 2011.

25. Livak KJ and Schmittgen TD: Analysis of relative gene expression data using real-time quantitative PCR and the 2(-Delta Delta C(T)) method. Methods 25: 402-408, 2001.

26. MacArthur Clark JA and Sun D: Guidelines for the ethical review of laboratory animal welfare People's Republic of China National Standard GB/T 35892-2018 [Issued 6 February 2018 Effective from 1 September 2018]. Animal Model Exp Med 3: 103-113, 2020.

27. Kilkenny C, Browne W, Cuthill IC, Emerson M and Altman DG; NC3Rs Reporting Guidelines Working Group: Animal research: Reporting in vivo experiments: the ARRIVE guidelines. J Gene Med 12: 561-563, 2010.

28. Norman D, Reis D, Zinman C, Misselevich I and Boss JH: Vascular deprivation-induced necrosis of the femoral head of the rat. An experimental model of avascular osteonecrosis in the skeletally immature individual or Legg-Perthes disease. Int J Exp Pathol 79: 173-181, 1998.

29. Yu R, Ma C, Li G, Xu J, Feng D and Lan X: Inhibition of toll-like receptor 4 signaling pathway accelerates the repair of avascular necrosis of femoral epiphysis through regulating macrophage polarization in Perthes disease. Tissue Eng Regen Med 20: 489-501, 2023.

30. Hawkins P, Armstrong R, Boden T, Garside P, Knight K, Lilley E, Seed M, Wilkinson M and Williams RO: Applying refinement to the use of mice and rats in rheumatoid arthritis research. Inflammopharmacology 23: 131-150, 2015.

31. Katri A, Dąbrowska A, Löfvall H, Ding M, Karsdal MA, Andreassen KV, Thudium CS and Henriksen K: Combining naproxen and a dual amylin and calcitonin receptor agonist improves pain and structural outcomes in the collagen-induced arthritis rat model. Arthritis Res Ther 21: 68, 2019.

32. Sun H, Zhang H, Li K, Wu H, Zhan X, Fang F, Qin Y and Wei Y: ESM-1 promotes adhesion between monocytes and endothelial cells under intermittent hypoxia. J Cell Physiol 234: 1512-1521, 2019.

33. Moreno Grangeiro P, Rodrigues JC, de Angeli LRA, Leão Filho H, Montenegro NB, Guarniero R, Dempsey M and Kim HKW: Feasibility of magnetic resonance angiography in patients with Legg-Calvé-Perthes disease. J Pediatr Orthop 41: e774-e779, 2021.

34. Kumar V, Ali S, Verma V and Singh A: Do bisphosphonates alter the clinico-radiological profile of children with Perthes disease? A systematic review and meta-analysis. Eur Rev Med Pharmacol Sci 25: 4875-4894, 2021.

35. Kuroyanagi G, Adapala NS, Yamaguchi R, Kamiya N, Deng Z, Aruwajoye O, Kutschke M, Chen E, Jo C, Ren Y and Kim HKW: Interleukin-6 deletion stimulates revascularization and new bone formation following ischemic osteonecrosis in a murine model. Bone 116: 221-231, 2018.

36. Lugo-Gavidia LM, Burger D, Matthews VB, Nolde JM, Galindo Kiuchi M, Carnagarin R, Kannenkeril D, Chan J, Joyson A, Herat LY, *et al*: Role of microparticles in cardiovascular disease: Implications for endothelial dysfunction, thrombosis, and inflammation. Hypertension 77: 1825-1844, 2021.

37. Yuana Y, Sturk A and Nieuwland R: Extracellular vesicles in physiological and pathological conditions. Blood Rev 27: 31-39, 2013.

38. Jimenez JJ, Jy W, Mauro LM, Soderland C, Horstman LL and Ahn YS: Endothelial cells release phenotypically and quantitatively distinct microparticles in activation and apoptosis. Thromb Res 109: 175-180, 2003.

39. Hu X, Barnum SR, Wohler JE, Schoeb TR and Bullard DC: Differential ICAM-1 isoform expression regulates the development and progression of experimental autoimmune encephalomyelitis. Mol Immunol 47: 1692-1700, 2010.

40. Kesanakurti D, Chetty C, Rajasekhar Maddirela D, Gujrati M and Rao JS: Essential role of cooperative NF-κB and Stat3 recruitment to ICAM-1 intronic consensus elements in the regulation of radiation-induced invasion and migration in glioma. Oncogene 32: 5144-5155, 2013.

41. Bonan S, Albrengues J, Grasset E, Kuzet S, Nottet N, Bourget I, Bertero T, Mari B, Meneguzzi G and Gaggioli C: Membrane-bound ICAM-1 contributes to the onset of proinvasive tumor stroma by controlling acto-myosin contractility in carcinoma-associated fibroblasts. Oncotarget 8: 1304-1320, 2017.

42. Kim JY, Kim DH, Kim JH, Lee D, Jeon HB, Kwon SJ, Kim SM, Yoo YJ, Lee EH, Choi SJ, *et al*: Soluble intracellular adhesion molecule-1 secreted by human umbilical cord blood-derived mesenchymal stem cell reduces amyloid-β plaques. Cell Death Differ 19: 680-691, 2012.

43. Li CH, Liao PL, Shyu MK, Liu CW, Kao CC, Huang SH, Cheng YW and Kang JJ: Zinc oxide nanoparticles-induced intercellular adhesion molecule 1 expression requires Rac1/Cdc42, mixed lineage kinase 3, and c-Jun N-terminal kinase activation in endothelial cells. Toxicol Sci 126: 162-172, 2012.

44. Bui TM, Wiesolek HL and Sumagin R: ICAM-1: A master regulator of cellular responses in inflammation, injury resolution, and tumorigenesis. J Leukoc Biol 108: 787-799, 2020.

45. Cook-Mills JM, Marchese ME and Abdala-Valencia H: Vascular cell adhesion molecule-1 expression and signaling during disease: Regulation by reactive oxygen species and antioxidants. Antioxid Redox Signal 15: 1607-1638, 2011.

46. Meigs JB, Hu FB, Rifai N and Manson JE: Biomarkers of endothelial dysfunction and risk of type 2 diabetes mellitus. JAMA 291: 1978-1986, 2004.

47. Dessein PH, Joffe BI and Singh S: Biomarkers of endothelial dysfunction, cardiovascular risk factors and atherosclerosis in rheumatoid arthritis. Arthritis Res Ther 7: R634-R643, 2005.

48. Li C, Zhang Y, Liu R and Mai Y: Anagliptin protected against hypoxia/reperfusion-induced brain vascular endothelial permeability by increasing ZO-1. ACS Omega 6: 7771-7777, 2021.

49. Urquiza-Fornovi I, Redondo-Alamillos M, García-Recuero I and Romance-García A: Mandible fracture in a child with osteogenesis imperfecta on bisphosphonates. Open versus closed treatment? A case report. Dent Traumatol 36: 692-696, 2020.

50. Malmgren B, Tsilingaridis G, Monsef-Johansson N, Qahtani ZHA, Dahllöf G and Åström E: Bisphosphonate therapy and tooth development in children and adolescents with osteogenesis imperfecta. Calcif Tissue Int 107: 143-150, 2020.

51. Nasomyont N, Hornung LN and Wasserman H: Intravenous bisphosphonate therapy in children with spinal muscular atrophy. Osteoporos Int 31: 995-1000, 2020.

52. Chen YP, Tan A, Ho WP, Chuang TY, Chen C and Chen CH: Effectiveness of strontium ranelate in the treatment of rat model of Legg-Calve-Perthes disease. Indian J Orthop 52: 380-386, 2018.

53. Ming X, Ding M, Zhai B, Xiao L, Piao T and Liu M: Biochanin A inhibits lipopolysaccharide-induced inflammation in human umbilical vein endothelial cells. Life Sci 136: 36-41, 2015.

54. Oh JS, Cho IA, Kang KR, You JS, Yu SJ, Lee GJ, Seo YS, Kim CS, Kim DK, Kim SG, et al: Biochanin-A antagonizes the interleukin-1β-induced catabolic inflammation through the modulation of NFκB cellular signaling in primary rat chondrocytes. Biochem Biophys Res Commun 477: 723-730, 2016.

55. Li Y, Dong J, Shang Y, Zhao Q, Li P and Wu B: Anti-inflammatory effects of hederagenin on diabetic cardiomyopathy via inhibiting NF-κB and Smads signaling pathways in a type-2 diabetic mice model. RSC Adv 9: 26238-26247, 2019.

56. Wang J, Wu ML, Cao SP, Cai H, Zhao ZM and Song YH: Cycloastragenol ameliorates experimental heart damage in rats by promoting myocardial autophagy via inhibition of AKT1-RPS6KB1 signaling. Biomed Pharmacother 107: 1074-1081, 2018.

57. Li ZH, Shi Z, Tang S, Yao HP, Lin X and Wu F: Epigallocatechin-3-gallate ameliorates LPS-induced inflammation by inhibiting the phosphorylation of Akt and ERK signaling molecules in rat H9c2 cells. Exp Ther Med 20: 1621-1629, 2020.

58. Xi Y, Miao Y, Zhou R, Wang M, Zhang F, Li Y, Zhang Y, Yang H and Guo F: Exploration of the specific pathology of HXMM tablet against retinal injury based on drug attack model to network robustness. Front Pharmacol 13: 826535, 2022.

59. Feng L, Zhu MM, Zhang MH, Wang RS, Tan XB, Song J, Ding SM, Jia XB and Hu SY: Protection of glycyrrhizic acid against AGEs-induced endothelial dysfunction through inhibiting RAGE/NF-κB pathway activation in human umbilical vein endothelial cells. J Ethnopharmacol 148: 27-36, 2013.

60. Zhu J, Xu Y, Ren G, Hu X, Wang C, Yang Z, Li Z, Mao W and Lu D: Tanshinone IIA Sodium sulfonate regulates antioxidant system, inflammation, and endothelial dysfunction in atherosclerosis by downregulation of CLIC1. Eur J Pharmacol 815: 427-436, 2017.

61. Li MT, Ke J, Guo SF, Wu Y, Bian YF, Shan LL, Liu QY, Huo YJ, Guo C, Liu MY, et al: The protective effect of quercetin on endothelial cells injured by hypoxia and reoxygenation. Front Pharmacol 12: 732874, 2021.

62. Yamaguchi R, Kamiya N, Kuroyanagi G, Ren Y and Kim HKW: Development of a murine model of ischemic osteonecrosis to study the effects of aging on bone repair. J Orthop Res 39: 2663-2670, 2021.

63. Kamiya N, Yamaguchi R, Aruwajoye O, Adapala NS and Kim HKW: Development of a mouse model of ischemic osteonecrosis. Clin Orthop Relat Res 473: 1486-1498, 2015.